JOURNAL OF MATERIALS SCIENCE 28 (1993) 1211–1219

Dielectric relaxation in $Ba(Ti_{0.8}Zr_{0.2})O_3$ ceramics prepared from sol–gel and solid state reaction powders

S. KAZAOUI, J. RAVEZ
Laboratoire de Chimie du Solide du CNRS, Université Bordeaux I, 351 cours de la Libération, 33405 Talence Cedex, France

In order to correlate dielectric relaxation properties with chemical homogeneity and microstructure in ferroelectric ceramics, powders are prepared both by sol–gel route and solid-state reaction. This comparative study concerns $Ba(Ti_{0.8}Zr_{0.2})O_3$ ceramics, with maximum permittivity close to room temperature. Dielectric relaxation is reported in the frequency and temperature ranges 10^6 to 10^9 Hz and 250–350 K, respectively. A minimum of the relaxation frequency occurs close to the phase transition temperature. The variations of f_r are correlated with chemical homogeneity and microstructure.

1. Introduction

The determination of the origin of the dielectric relaxation observed in $BaTiO_3$ crystals and ceramics around 10^8 Hz is in progress but still relatively discussed [1]. Several theoretical attempts including intrinsic and extrinsic mechanisms have been taken into account. A similar dielectric relaxation has also been observed in solid solutions with composition $Ba(Ti_{1-x}Zr_x)O_3$, $Ba(Ti_{1-x}Hf)_xO_3$ and $(Ba_{1-y}Sr_y)TiO_3$ (x and $y \leq 0.3$) [2, 3].

The purpose of the present work is to determine the influence of chemical homogeneity and microstructure on the dielectric relaxation characteristics. $Ba(Ti_{0.8}Zr_{0.2})O_3$ ceramics prepared from either sol–gel or solid-state reaction powders have been chosen because the phase transition temperature is close to room temperature.

2. Chemical processing of $Ba(Ti_{0.8}Zr_{0.2})O_3$ perovskite ceramics

2.1. Powder preparation

In the past few years the sol–gel method (SG) has been widely studied as a new route for the preparation of ceramics. Some of the advantages of the sol–gel method are: the mixing of reactants on a molecular level, a better control of the stoichiometry, higher-purity raw materials, the easy formation of ultrafine and crystallized powders. We have prepared powders of $Ba(Ti_{0.8}Zr_{0.2})O_3$ from the sol–gel route, as previously proposed by Kiss *et al.* [4] for barium titanate and recently by Chaput and Boilot [5], in which titanium and zirconium alkoxides are hydrolysed by barium hydroxide in alcohol solution. Fig. 1 describes the two preparation methods of perovskite powders by alkoxide–hydroxide and conventional methods. The organic mixture containing $Ti(OC_3H_7)_4$ and $Zr(OC_3H_7)_4$ in stoichiometric proportions is hydrolysed/condensed, at about 80 °C, by an alcohol solution (2-butanol) containing $Ba(OH)_2 \cdot 8H_2O$. Reactions which take place have been previously described by Flaschen [6] for barium titanate and extended to titanozirconate. After reaction, the precipitate containing water and alcohol is dried under vacuum at 80 °C. The reaction is

$$(1-x)Ti(OC_3H_7)_4 + xZr(OC_3H_7)_4 + Ba^{2+} + 4H_2O + 2OH^- \rightarrow Ba(Ti_{1-x}Zr_x)O_3 + 4C_3H_7OH + 3H_2O$$

X-ray diffraction patterns of the dried powder and of samples treated at various temperatures are characteristic of a perovskite phase (Fig. 2a). The degree of crystallinity appears relatively good above 750 °C (narrow diffraction lines). According to thermogravimetric analysis (TGA) performed with a rate of 5 °C min^{-1} a weight loss of less than 5% appears in the range 50–400 °C and slightly decreases from 400 up to 950 °C (Fig. 3a). It can be attributed to the departure, by volatilization, of organic solvant (2-butanol), water vapour and n-propoxide (C_3H_7OH), products of the reaction. This assumption is confirmed by pyrolysis coupled to gaseous phase chromatography and mass spectrometry from 50 to 1000 °C (Fig. 3b).

A weak ionic current appears corresponding to H_2O and to alcohol departure. The i.r. absorption spectra of $Ba(Ti_{0.8}Zr_{0.2})O_3$ with increasing heat treatment show that the absorption band at 3400 cm^{-1} (stretching O–H) becomes weaker and vanishes at 750 °C, whereas the bands at 576 and 400 cm^{-1} become stronger (Fig. 2b). These latter correspond to the characteristic peaks of $BaTiO_3$ as previously reported by Last [7]. In contrast to the sol–gel route, the

0022–2461

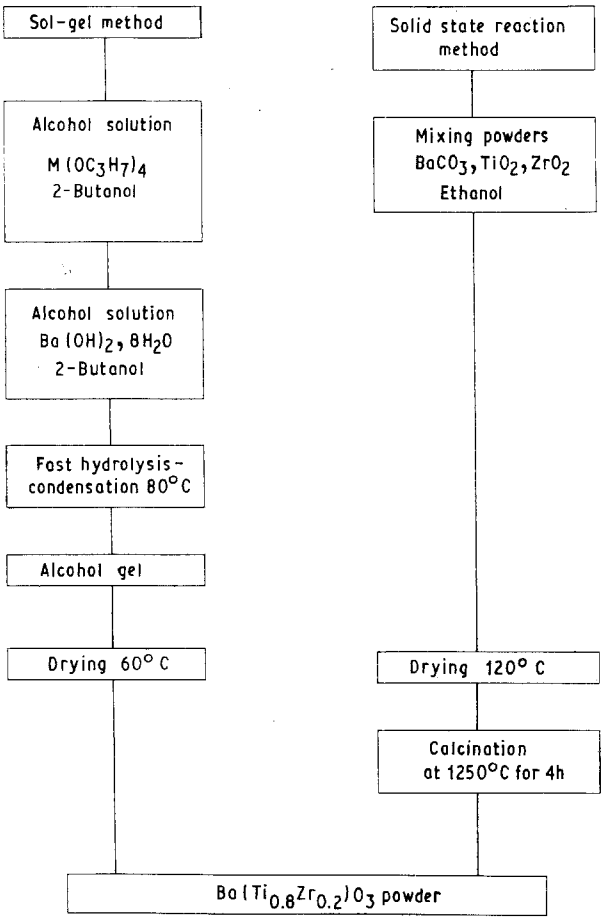

Figure 1 Powder preparation by sol–gel or solid-state reaction methods.

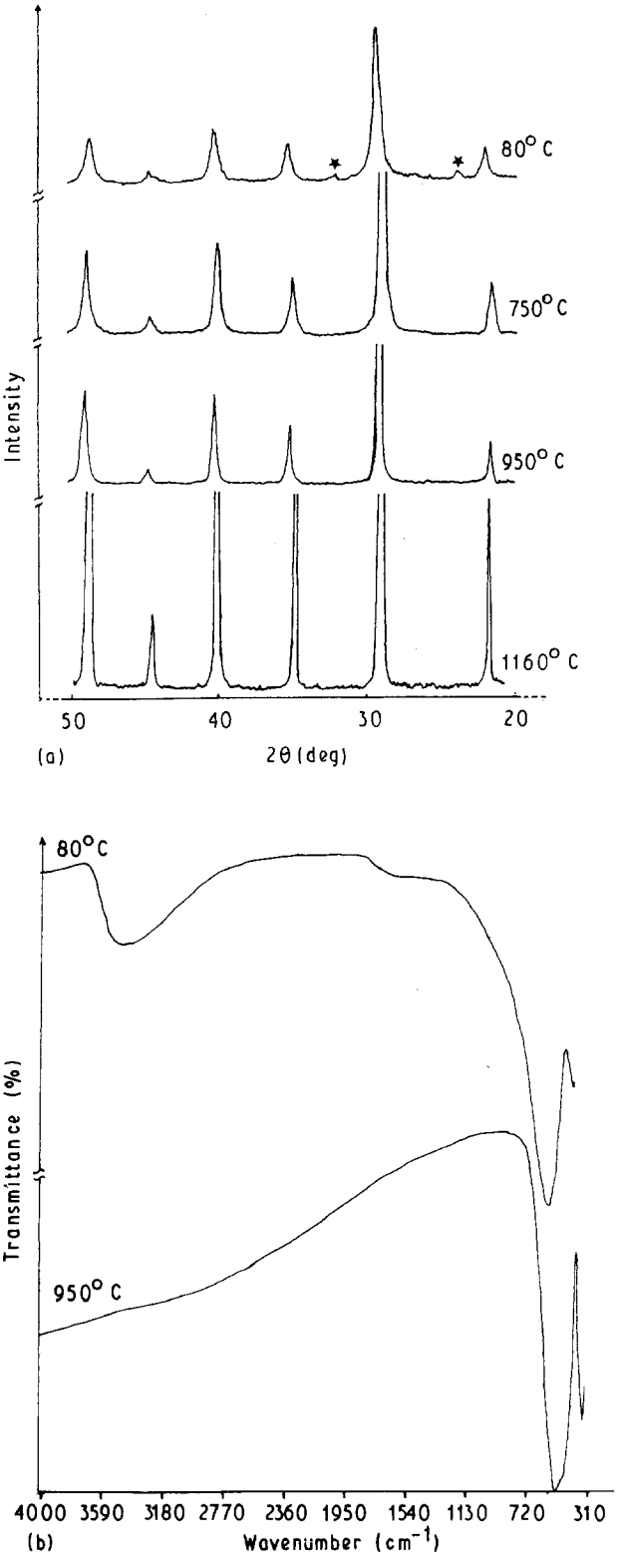

Figure 2 (a) X-ray diffraction patterns (CuK_α) and (b) i.r. spectra for SG powders at various temperatures. (★) $BaCO_3$.

conventional solid–state reaction method (SSR) requires higher calcination temperatures. Such powders are prepared from $BaCO_3$, TiO_2 and ZrO_2, in stoichiometric proportions, at 1250 °C for 4 h. The degree of crystallinity appears relatively good (narrow diffraction lines) and the X-ray diffraction pattern corresponds to a perovskite phase:

$$BaCO_3 + (1 - x)TiO_2 + xZrO_2 \rightarrow Ba(Ti_{1-x}Zr_x)O_3 + CO_2$$

2.2. Ceramic preparation

The sintering ability of ceramics has been tested for both SG and SSR powders. The average grain sizes of the desagglomerated sol–gel powders and of the crushed SSR one are respectively 0·3 and 2 μm. The powders were pressed into discs of 6 mm diameter and about 1.5 mm thickness. Dilatometric curves indicate clearly that the sintering begins at 1100 and 1200 °C from SG and SSR powders, respectively (Fig. 4). The better sinterability of sol–gel powders as a result of ultrafine particle size and lower temperature of crystallization leads to a lower sintering temperature and higher densification kinetics. The shrinkage is maximum at 1300 and 1450 °C from SG and SSR powders, respectively.

Sol–gel derived powders were sintered under an oxygen atmosphere either at 1300 °C for various times (1, 15, 30, 45, 60 and 120 min) or for 2 h at different temperatures (1290, 1300 and 1320 °C). Conventional SSR-derived powders were sintered at 1450 °C for 4 h under an oxygen atmosphere. The oxygen atmosphere is used to prevent the formation of ionic defects during sintering.

SEM analyses were performed after mechanical polishing and thermal etching of ceramics (Fig. 5). Table I presents the microstructure parameters: average grain size ϕ_g, grain size distribution $\Delta\phi_g$, compactness C and porosity. Highly densified SG ceramics ($C \simeq 0.95$) sintered at 1300 °C for 1 to 45 min have

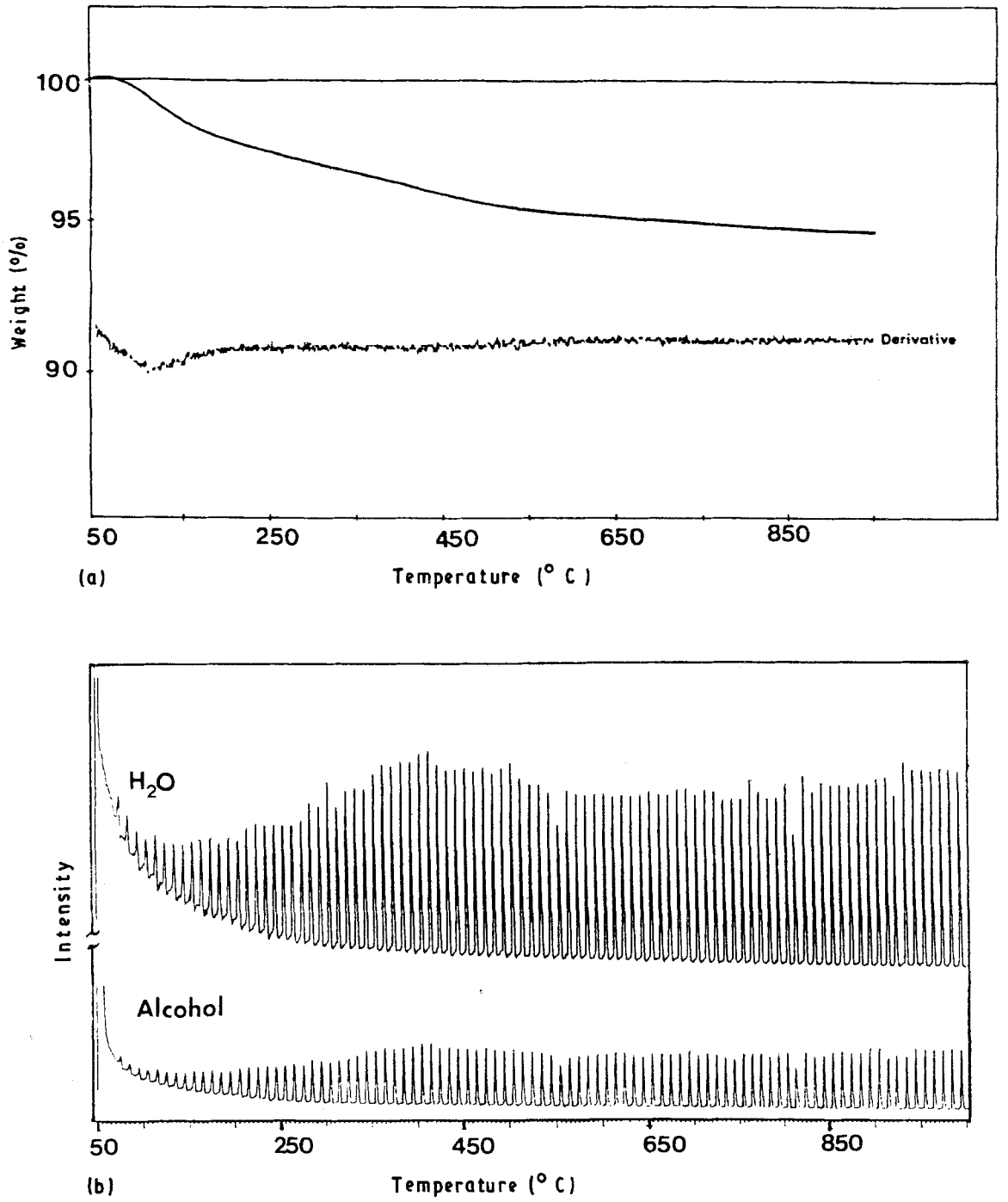

Figure 3(a) TGA and (b) ionic current curves for SG powder. Weight change = 5.19% from 50 to 950 °C.

grain sizes in the range 4 to 8 μm. Sintering temperatures over 1300 °C and/or times greater than 45 min revealed samples with large grains ($\phi_g \geq 25$ μm), a wide grain size distribution, lower compactness ($C \simeq 0.92$) and higher porosity. The excessive grain growth might be correlated with a larger mobility of the grain boundaries due to the better chemical homogeneity. Conventional ceramics (SSR), sintered at higher temperatures, are characterized by an average grain size of 15 μm, a large grain size distribution, high compactness ($C \simeq 0.95$) and low porosity.

3. Dielectric studies

3.1. Experimental procedure

Gold electrodes were deposited on both disc faces of the ceramics by sputtering. The capacitance and the dissipation factor were firstly measured at 10^3 Hz in the range 150–450 K using a capitance bridge WK 6425. The temperature dependence of ε_r showed a maximum at each transition temperature. The permittivities ε'_r and ε''_r were then measured at high frequencies from 10^6 to 10^9 Hz, using a network analyser HP 8753 A, and at various temperatures in the range 250–350 K. Broad-band analysis of a coaxial line loaded with the disc sample (diameter 7 mm) and backed up by a short circuit enabled us to calculate the complex permittivity from complex impedance measurements [8, 9]. The curves for ε'_r and ε''_r versus frequency allow the determination of relaxation frequency f_r, ε'_s (permittivity at $f \ll f_r$), ε'_∞ (permittivity at $f \gg f_r$) and α (relaxation time distribution).

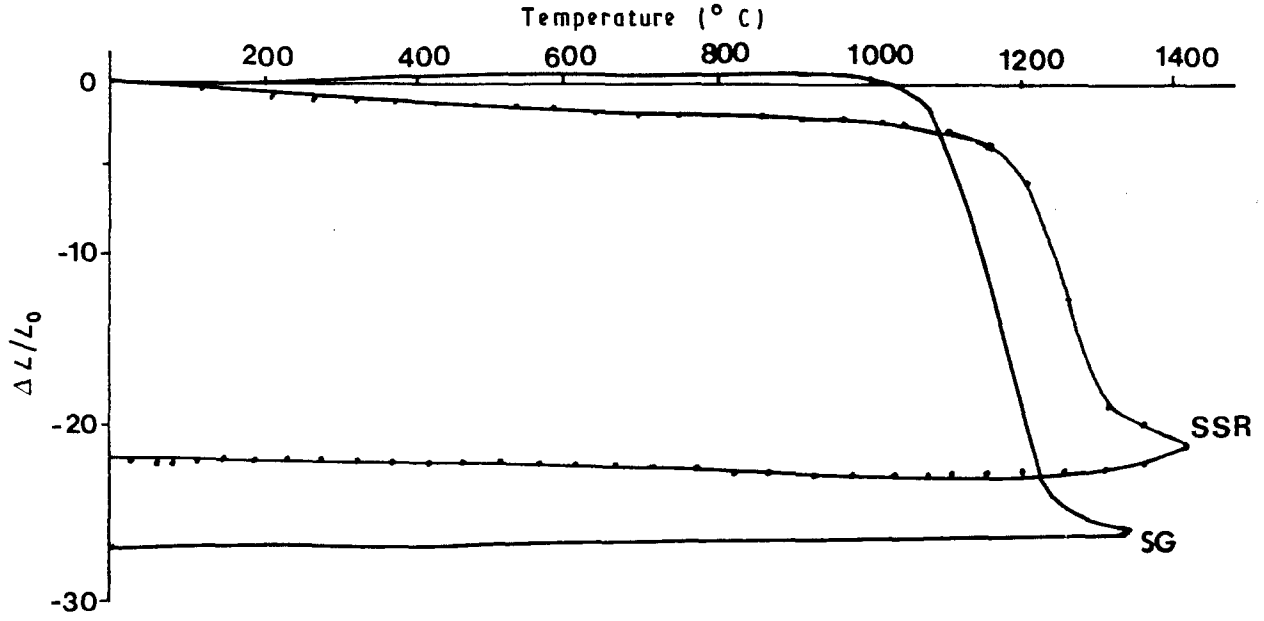

Figure 4 Dilatometric curves from SG and solid-state reaction powders.

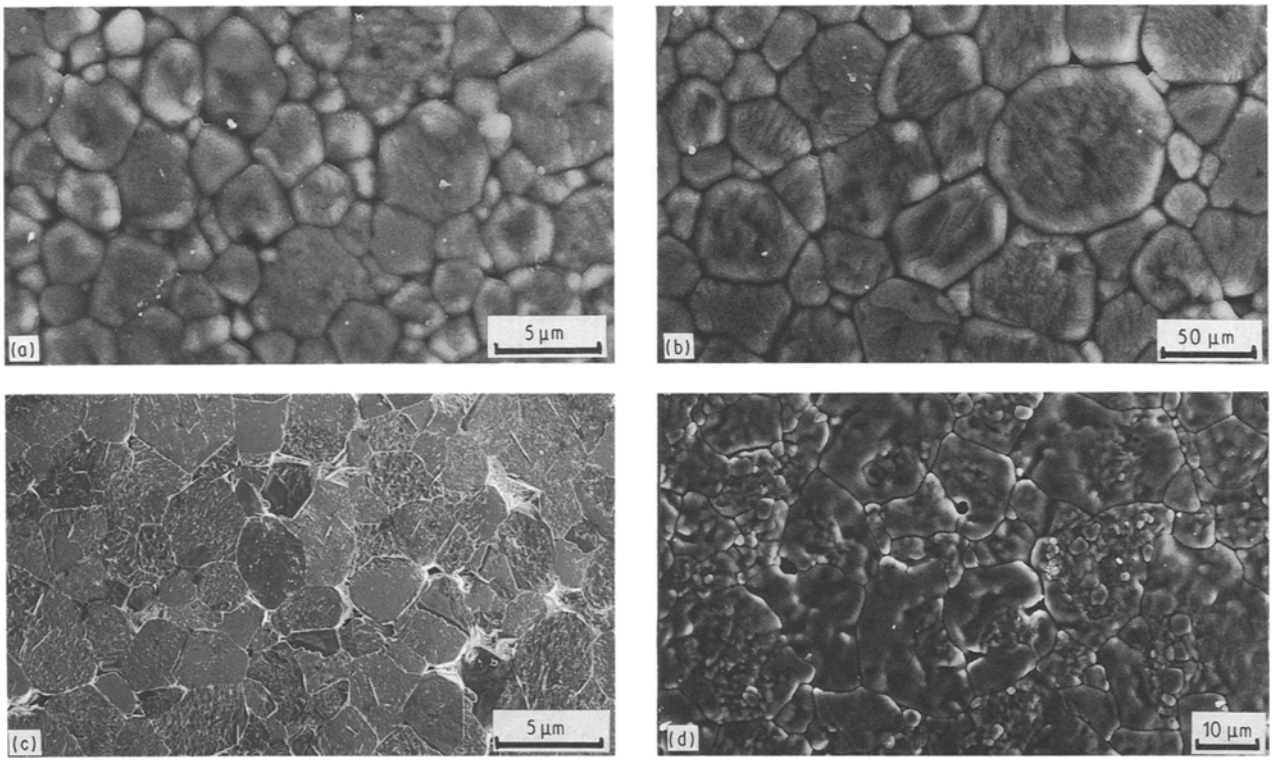

Figure 5 Scanning electron micrographs of ceramics. SG ceramics sintered at 1300 °C for (a) 1 min and (b) 45 min, and (c) at 1320 °C for 2 h; (d) SSR ceramic sintered at 1450 °C for 4 h.

TABLE I Microstructure parameters of SG ceramics sintered under oxygen atmosphere: average grain size ϕ_g, grain size distribution $\Delta\phi_g$, compactness and porosity

$T_{sint.}$ (°C)	$t_{sint.}$ (°C)	ϕ_g (µm)	$\Delta\phi_g$	Compactness	Porosity
1300	1 min	4	Narrow	0.95	Weak
1300	15 min	4	Narrow	0.94	Weak
1300	30 min	8	Narrow	0.94	Weak
1300	45 min	8	Medium	0.96	Weak
1300	1 h	10	Medium	0.92	Weak
1300	2 h	25	Large	0.93	Medium
1290	2 h	15	Large	0.92	Medium
1300	2 h	25	Large	0.93	Medium
1320	2 h	25	Large	0.92	Medium

3.2. Dielectric measurements at low frequency

Fig. 6 shows some typical results of dielectric measurements: the thermal dependence of ε'_r, $\tan\delta$ and $1/\varepsilon'_r$. The Curie temperature phase transition, dielectric constant and dissipation factor of ceramics prepared from either SG or SSR powders are found to depend markedly on the degree of chemical homogeneity and on sintering conditions (temperature, dwell time and atmosphere). The data indicate that homogeneous $Ba(Ti_{0.8}Zr_{0.2})O_3$ ceramics prepared by the sol–gel route (curves 1, 2 and 3) have a lower Curie temperature ($T_C = 305$ K) compared with that prepared by the SSR method (curve 4) ($T_C = 315$ K). This decrease of T_C from 315 to 305 K is probably due to the greater reactivity of SG powders. The slow reaction and diffusion of the more refractory constituent ZrO_2, in the SSR method are the major factors which inhibit the substitution of Ti^{4+} by Zr^{4+}, leading to the decrease of T_C [10, 11]. The diffuse character of the phase transition is correlated with the chemical homogeneity of the ceramics and thus with composition fluctuation due to statistical distribution of the various cations: $\varepsilon'_r > 15 \times 10^3$ (SG) whereas $\varepsilon'_r < 10^3$ (SSR). Comparison with the dielectric properties of ceramics obtained by the sol–gel method outlines the purely microstructure effects (curves 1, 2 and 3) such as grain size and compactness.

3.3. Dielectric measurements at high frequency

In order to correlate dielectric relaxation properties with microstructure and chemical homogeneity, hyperfrequency measurements were carried out on ferroelectric ceramics prepared by either sol–gel or conventional methods. Fig. 7 shows as an example the frequency and temperature dependences of ε'_r or ε''_r for a sol–gel ceramic sintered at 1300 °C for 1 min. Fig. 8 presents only the temperature dependence of the dielectric constants ε' and ε'' at various frequencies. The

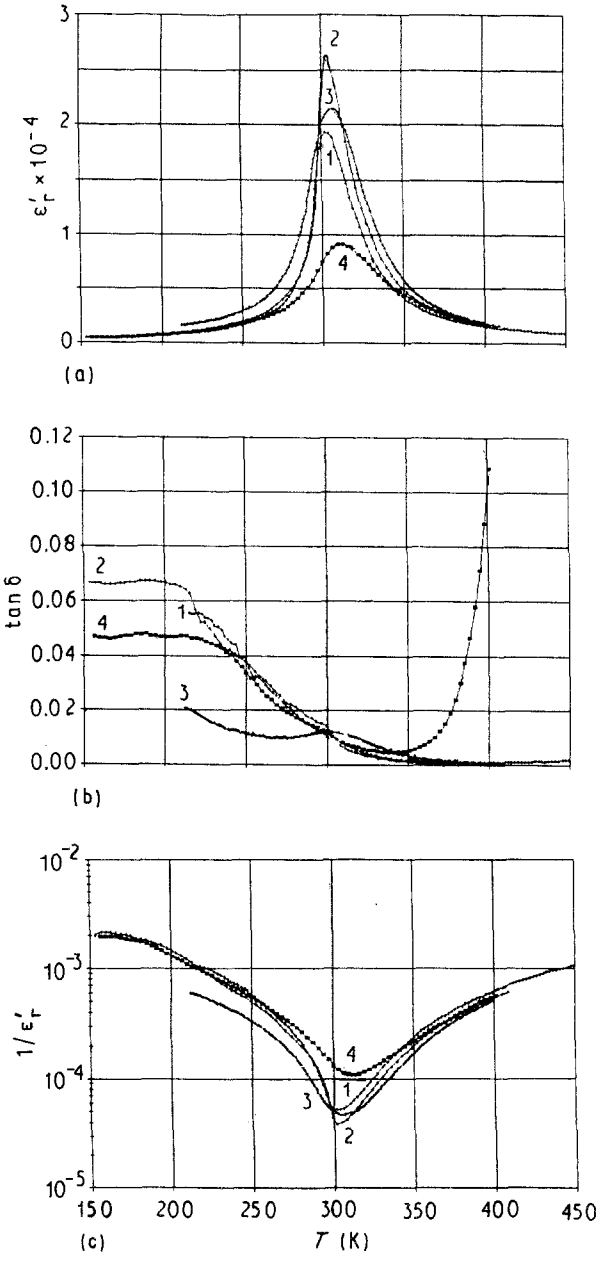

Figure 6 (a) ε'_r, (b) $\tan\delta$ and (c) $1/\varepsilon'_r$ versus temperature for SG ceramics sintered at 1300 °C for (1) 1 min, (2) 45 min, and (3) at 1320 °C for 2 h, (4) SSR ceramic sintered at 1450 °C for 4 h.

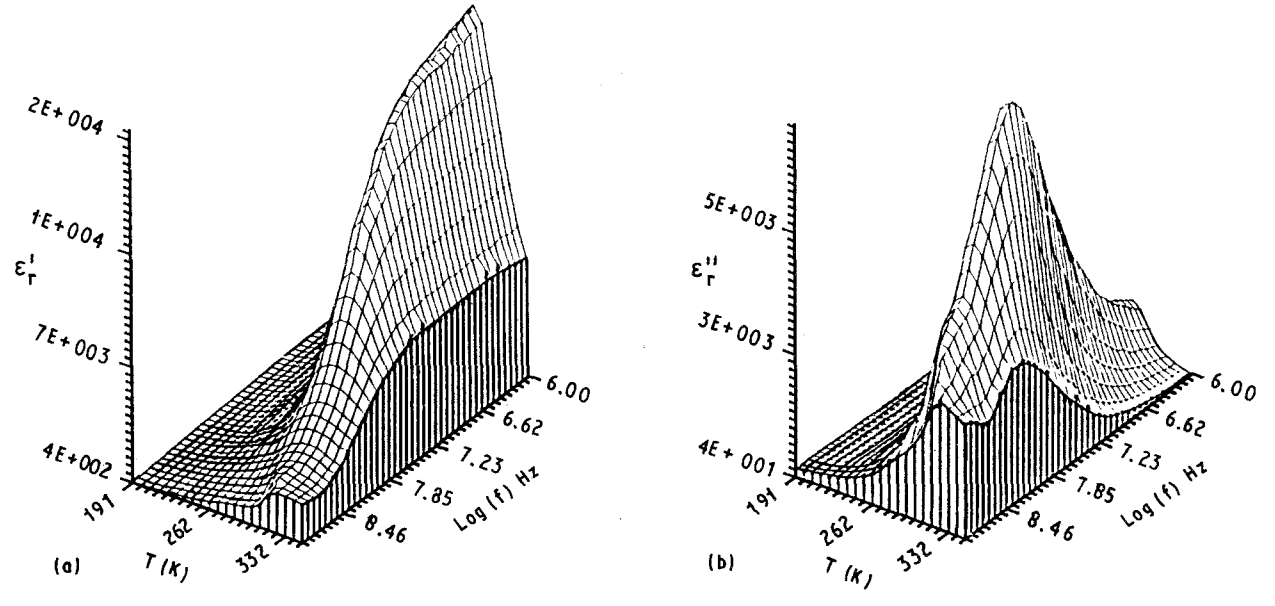

Figure 7 (a) ε'_r and (b) ε''_r versus frequency and temperature for an SG ceramic sintered at 1300 °C for 1 min.

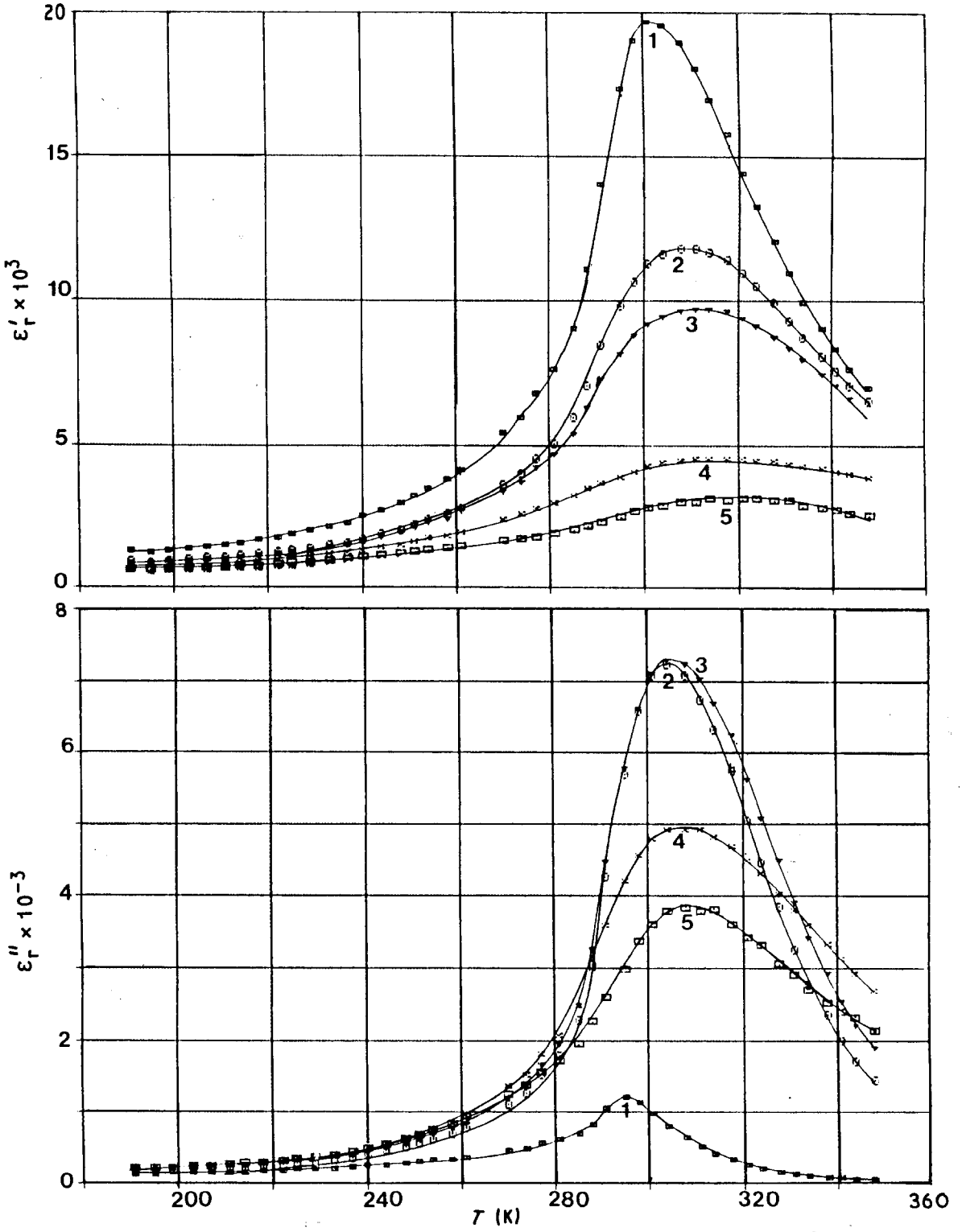

Figure 8 (a) ε'_r and (b) ε''_r versus temperature at various frequencies for an SG ceramic sintered at 1300 °C for 1 min: (1) 10^6 Hz, (2) 5×10^7 Hz, (3) 7×10^7 Hz, (4) 2×10^8 Hz, (5) 4×10^8 Hz.

dielectric constant ε'_r at 10^6 Hz shows a sharp maximum at the Curie temperature $T_C = 305$ K. The dielectric constant $\varepsilon'_r(T)$ measured at 10^6 Hz is regarded as the static dielectric constant ε'_s with a value close to that obtained at 10^3 Hz. As one can see, $\varepsilon'_r(T)$ has a pronounced frequency dependence near the ferroelectric phase transition. As the frequency increases, ε'_r decreases, the peak of ε'_r shifts to a higher temperature and it broadens out. The dielectric constant ε''_r also presents a maximum close to T_C. On increasing the frequency, the value of ε''_{max} passes through a maximum for $f = 5 \times 10^7$ Hz and above this frequency it decreases and the peak becomes more diffuse. Figs 9 and 10 show the frequency dependence of ε'_r and ε''_r at various temperatures above and below $T_C = 305$ K. Such variations are characteristic of a dielectric relaxation. Argand diagrams, ε''_r (ε'_r) are drawn in order to characterize this relaxation (Fig. 10). The curves obtained are very close to circular arcs, in agreement with a Cole–Cole model. The complex permittivity ε^* is thus expressed by the formula [12]

$$\varepsilon^* = \varepsilon'_\infty + \frac{\varepsilon'_s - \varepsilon'_\infty}{1 + (if/f_r)^{1-\alpha}} \quad (1)$$

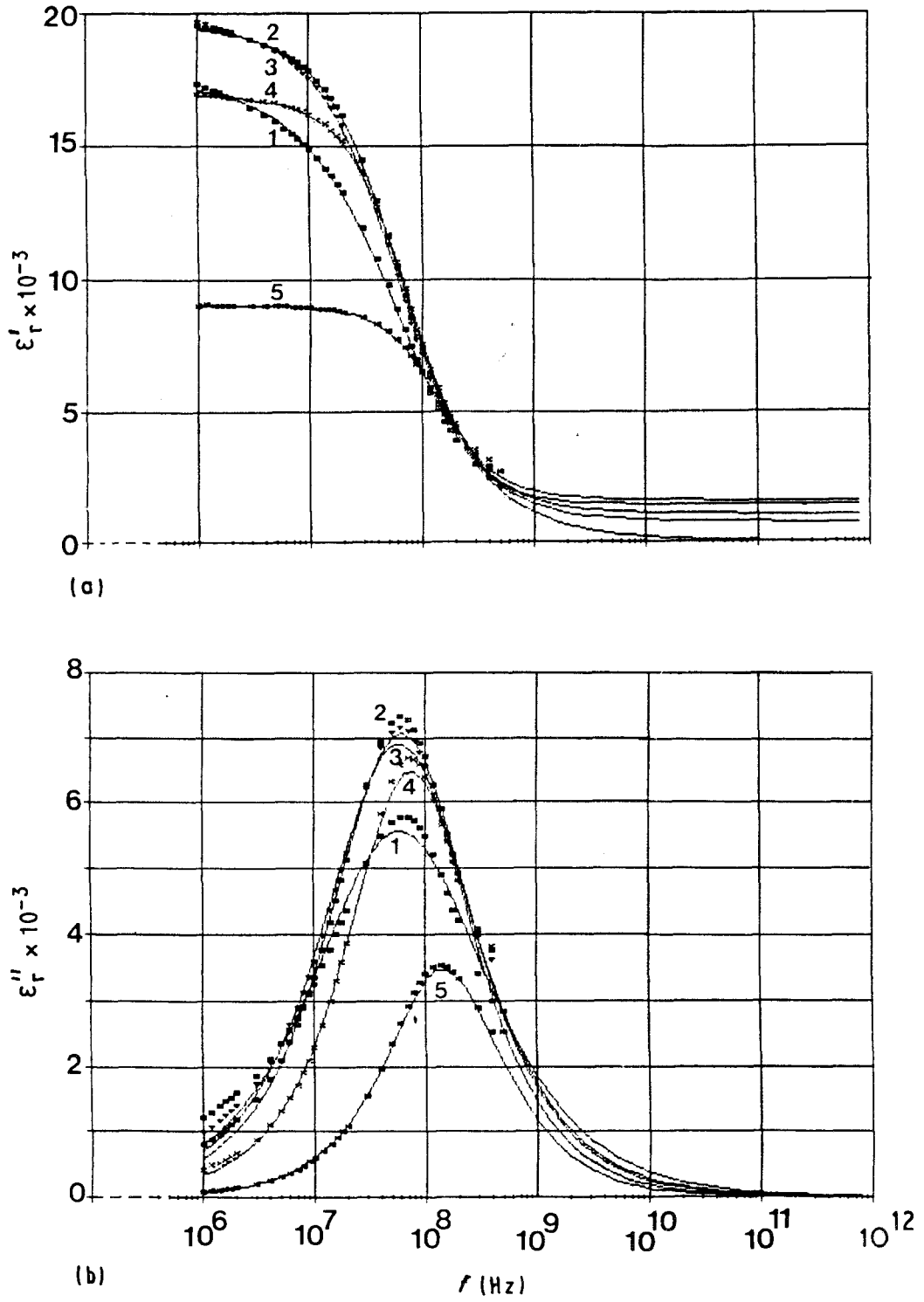

Figure 9 (a) ε'_r and (b) ε''_r versus frequency at various temperatures for an SG ceramic sintered at 1300 °C for 1 min: (■, ×) experimental points, (———) theoretical curves. (1) 295 K, (2) 301 K, (3) 304 K, (4) 314 K, (5) 334 K.

A relatively good agreement appears between experimental points and theoretical curves. A similar dielectric relaxation is observed for ceramics prepared by either SG or SSR route.

Fig. 11 illustrates the dependence of f_r on temperature for three samples. It is interesting to remark that dielectric dispersion occurs not only in the ferroelectric region but also in the paraelectric one at temperatures relatively close to T_C. For each ceramic a minimum of f_r appears close to the transition temperature; such a result has been previously reported for pure and iron-doped $BaTiO_3$ crystals [1] as well as for $BaTiO_3$, $Ba(Ti_{1-x}Hf_x)O_3$, $(Ba_{1-y}Ca_y)TiO_3$ and $(Ba_{1-y}Sr_y)TiO_3$ ceramics [2, 3, 13]. The temperature variation of f_r for each composition may be correlated with the microstructure and/or the chemical homogeneity of the ceramic. The more diffuse is the phase transition (see Fig. 6, $\varepsilon'_r(T)$ at 10^3 Hz), the broader is the $f_r(T)$ curve. As the diffuse phase transition is correlated with chemical homogeneity, thus $f_r(T)$ is also correlated with composition fluctuation due to statistical distribution of the different cations.

In addition hyperfrequency measurements were performed for two ceramics (SG) with average grain

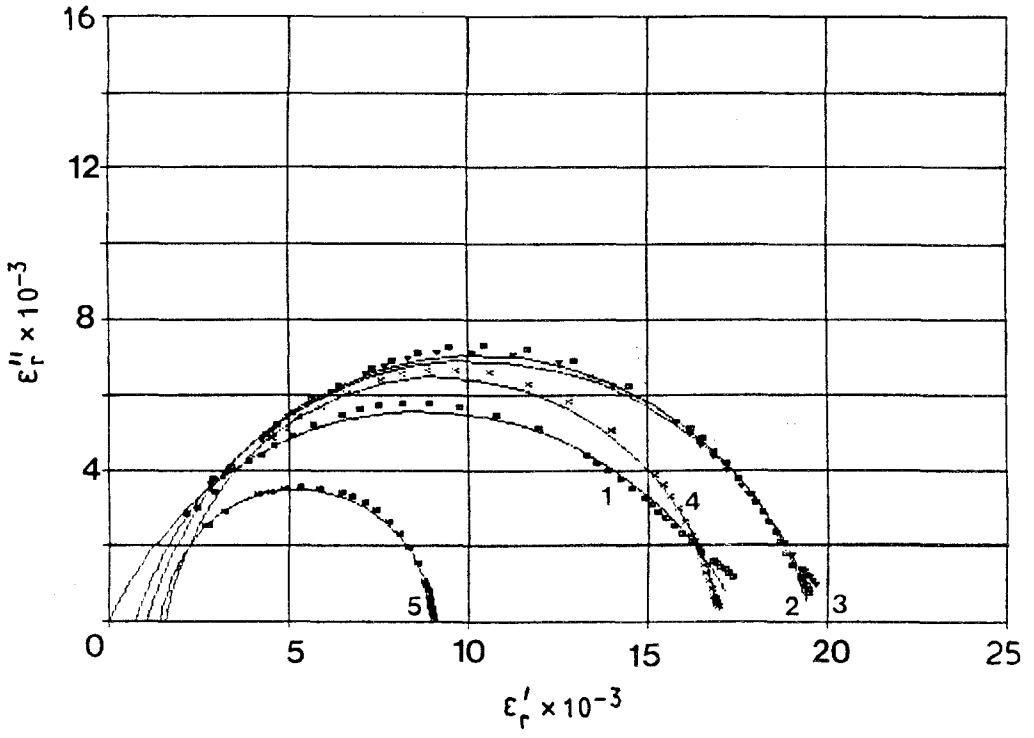

Figure 10 Argand diagram at various temperatures (see Fig. 9) for an SG ceramic sintered at 1300 °C for 1 min.

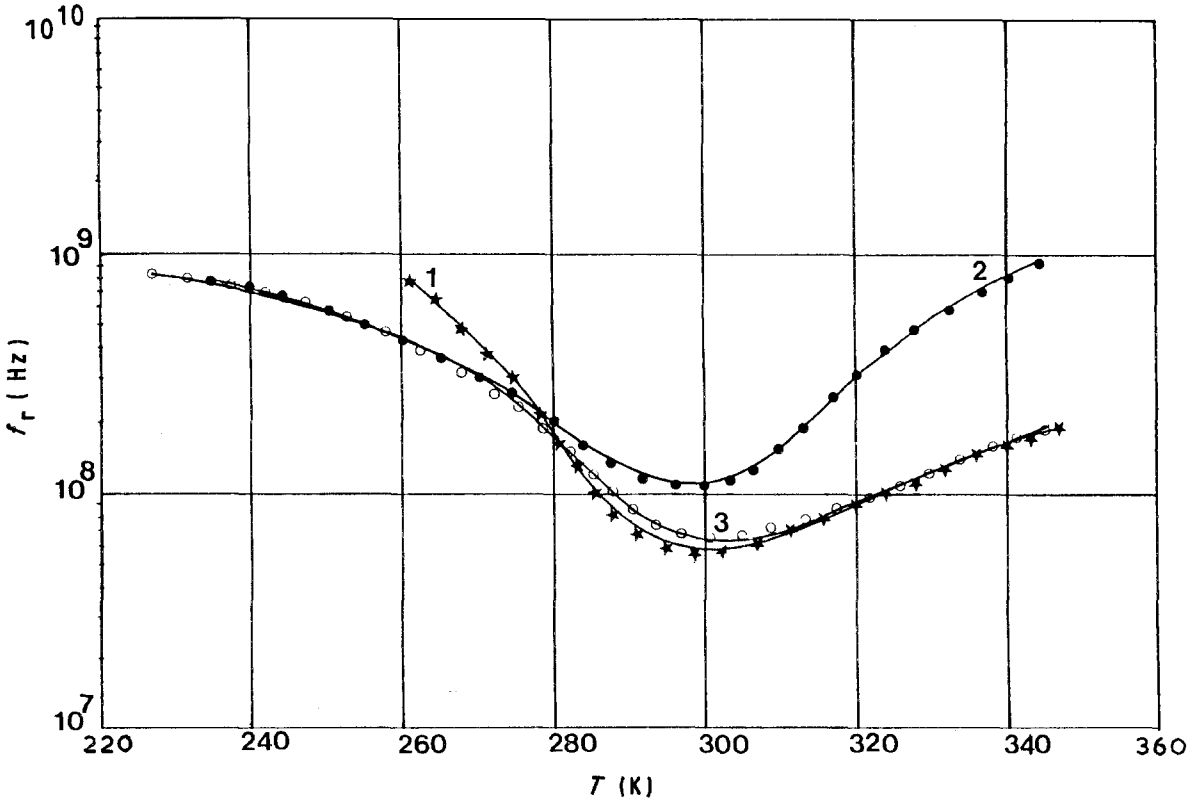

Figure 11 f_r versus temperature for (1) SG ceramic sintered at 1300 °C for 1 min, (2) SG ceramic sintered at 1320 °C for 2 h and (3) SSR ceramic sintered at 1450 °C for 4 h.

size 4 and 8 μm, respectively. The relaxation frequency is independent of the grain size and the value of the relaxation frequency is f_r (min.) = 5×10^7 Hz.

The difficulty of sintering to end-point density and porosity is a problem for high-frequency measurements. Two ceramics with compactness 0.95 and 0.92 respectively show a different relaxation frequency behaviour: the minimum of f_r is lower for the higher densified sample (5×10^7 Hz) than for the less densified one (10^8 Hz). In contrast, dielectric measurements carried out on $BaTiO_3$ single crystal and ceramic ($\phi_g \simeq 4$ μm and compactness 0.95) exhibit the same values for $f_{r(min)} = 1.5 \times 10^8$ Hz at T_C and f_r (300 K) = 5×10^8 Hz.

3.4. Discussion

The determination of the origin of the dielectric dispersion of such ferroelectric ceramics in the range 10^6–10^9 Hz is in progress but still relatively discussed. Several theoretical attempts including intrinsic and extrinsic mechanisms have been taken into account. Some authors have proposed piezoelectric domain resonance as a relaxation mechanism [14–17]. Piezoelectric measurements versus temperature have been performed on poled specimens when the temperature increases from ferroelectric to paraelectric region; the piezoelectric resonance amplitude decreases and completely disappears above T_C [18]. However, as mentioned before, dielectric dispersion is reported here on $Ba(Ti_{0.8}Zr_{0.2})O_3$ in both ferroelectric and paraelectric regions and is reversible on passing through T_C. Thus comparative piezoelectric and dielectric studies allow us to conclude that the dielectric dispersion is not correlated with piezoelectric resonance. An atomic approach is thus necessary to explain the dielectric dispersion mechanism. Developments in the microscopic description of ferroelectrics are due to the soft-mode concept applied by Cochran [19], Anderson [20] and Ginsburg [21]. Dielectric dispersion is probably correlated with the overdamped soft mode [22]. In another way, the lattice-dynamical basis of Devonshire's theory predicts that the soft mode varies with the temperature as the inverse of the permittivity ε'_r [22]:

$$\omega_0^2 = \frac{4\pi}{\varepsilon'_r m g^2 V_a} \qquad (2)$$

where ω_0 is the frequency of the TO modes, m the reduced mass of the ions which move, V_a the unit cell volume and $g = 3/(\varepsilon'_\infty + 2)Z_e^*$, where Z_e is the dynamic charge and ε'_∞ the permittivity at $f \gg f_r$. Substituting Equation 2 into $f_r = \omega_0/2\pi$, for the sake of simplicity the following equation can be given:

$$f_r = D(\varepsilon_r)^{-0.5} \qquad \text{where } D = (2\pi g^2 m V_a)^{-0.5}$$

The relaxation frequency is thus correlated with the inverse of the permittivity and thus with the polarization. Ferroelectricity in perovskite compounds is related with Ti atom displacements from the barycentre of the oxygen octahedron. As one can see, there is a strong similitude between the temperature dependences of both $1/\varepsilon'_r$ (Fig. 6) and f_r (Fig. 10) for each ceramic. The maximum of ε_r at T_C corresponds to the minimum of the relaxation frequency and to the maximum of the dispersion step $\Delta\varepsilon'_r = \varepsilon'_s - \varepsilon'_\infty$. Comparing sol–gel processing with the conventional solid-state reaction method, as was done in previous sections, it is expected that the sol–gel samples have purity and homogeneity higher than those prepared by conventional routes. It is observed that a higher chemical homogeneity results in a lower concentration of defects and a better statistical distribution of different atoms, which leads to a lower relaxation frequency and a less broad $f_r(T)$ curve.

4. Conclusion

The processing and dielectric properties of ferroelectric $Ba(Ti_{0.8}Zr_{0.2})O_3$ ceramics from the sol–gel route are presented and compared with those of ceramics prepared from solid-state reaction powders. This study allows us to examine the influence of chemical homogeneity and microstructure on dielectric properties at either low frequency (10^3 Hz) or high frequency (10^6–10^9 Hz). The results obtained on dielectric relaxation are in outline, as follows.

(i) A dielectric relaxation occurs around 10^8 Hz not only in the ferroelectric region but also in the paraelectric one close to the Curie point. Moreover a minimum of f_r appears close to the phase transition temperature.

(ii) The variations of $f_r(T)$ are correlated with chemical homogeneity but are not dependent on the ceramic grain size.

These results, associated with piezoelectric measurements, suggest the dielectric relaxation to be due to an intrinsic mechanism.

Acknowledgement

The authors wish to thank F. Duboudin for valuable discussions.

References

1. M. MAGLIONE, R. BÖHMER, A. LOIDL and U. T. HÖCHLI, *Phys. Rev. B* **40** (1989) 11441.
2. S. KAZAOUI and J. RAVEZ *Phys. Status Solidi (a)* **123** (1991) 165.
3. *Idem, ibid.* **125** (1991) 715.
4. K. KISS, J. MAGDER, VUKASOVICH and R. J. LOCKHART, *J. Amer. Ceram. Soc.* **49** (1966) 291.
5. F. CHAPUT and J. P. BOILOT, *J. Mater. Sci. Lett.* **6** (1987) 1110.
6. S. S. FLASCHEN, *J. Amer. Chem. Soc.* **77** (1955) 6194.
7. J. T. LAST, *Phys. Rev.* **105** (1957) 1740.
8. N. BELHADJ-TAHAR and A. FOURIER-LAMER, IEEE *Trans. Microwave Theory Techn.* **NTT 34** (1986) 346.
9. A. LARGETEAU and D. AVILES-CASTRO, *Mater. Res. Bull.* **25** (1990) I.
10. R. C. KELL and N. J. HELLICAR, *Acustica* **6** (1956) 235.
11. S. M. NEIRMAN, *J. Mater. Sci.* **23** (1988) 3973.
12. K. S. COLE and R. H. COLE, *J. Chem. Phys.* **43** (1941) 341.
13. S. KAZAOUI, J. RAVEZ and J. L. MIANE, in Proceedings, "Caractérisation microondes des matériaux absorbants", Limoges, (1991) 249.
14. C. KITTEL, *Phys. Rev.* **83** (1951) 458.
15. J. FOUSEK, *Czech. J. Phys.* **9** (1959) 172.
16. A. V. TURIK and N. B. SHEVCHENKO, *Phys. Status. Solidi (b)* **95** (1979) 585.
17. XI YAO, M. H. KINSTRI and L. E. CROSS, *J. Amer. Ceram. Soc.* **66** (1983) 637.
18. A. YU KUDZIN, L. K. BUNINA and O. A. GRZHEGORZHEVSKII, *Sov. Phys. Solid State* **11** (1970) 1939.
19. W. COCHRAN, *Phys. Rev. Lett.* **3** (1959) 412.
20. P. W. ANDERSON, in "Fizika Dielectrikov", edited by G. I. Skanavi (Acad. Nauk. SSR, Moscow, 1960) p. 290.
21. V. L. GINSBURG, *Fiz. Tverd. Tela.* **2** (1960) 2031.
22. P. BRÜESSCH, "Phonons: Theory and Experiments", Vol. 3 (Springer, Berlin, 1987).

Received 2 October 1991
and accepted 14 August 1992